Hydrothermal Synthesis of Single-Crystal Szaibelyite $MgBO_2(OH)$ Nanobelt as a New Host Material for Red-Emitting Rare-Earth Ions

Jinping Liu,*[,†] Yuanyuan Li,[†] Xintang Huang,*[,†‡] Zikun Li,[†] Guangyun Li,[†] and Haibo Zeng[§]

Department of Physics, Central China Normal University, Wuhan 430079, P. R. China; Key Laboratory of Ferroelectric and Piezoelectric Materials and Devices of Hubei Province, Hubei University, Wuhan 430062, P. R. China; and Key Laboratory of Materials Physics, Anhui Laboratory of Nanomaterials and Nanotechnology, Institute of Solid State Physics, Chinese Academy of Sciences, Hefei 230-031, Anhui P. R. China

Received September 22, 2007. Revised Manuscript Received November 11, 2007

A one-step template-free process for the fabrication of pure, doped, and codoped single-crystal $MgBO_2(OH)$ nanobelts in high yield has been presented. The growth mechanism of such novel nanobelts has been investigated on the basis of time-dependent experiments and the crystal structure of szaibelyite $MgBO_2(OH)$. Upon excitation with 260 nm ultraviolet light, Eu^{3+}-doped nanobelts show a dominant red emission (615 nm) that is visible to the naked eye, indicating that $MgBO_2(OH)$ is a new promising host material for the luminescence of rare-earth ions. With the introduction of Y^{3+} codopant, the emission intensities of all the peaks are efficiently enhanced and the intensity ratio (R) of 593 to 615 nm emissions increases. The reason for the spectral change relating to Y^{3+} modification is also discussed. The obtained red-emitting nanobelts which can be easily made into transparent thin film have great potential in a wide variety of applications such as transparent luminescent layers. The approach presented herein is expected to provide access to additional multicomponent functional nanobelts with or without dopants.

1. Introduction

Starting with the discovery of binary semiconducting oxide nanobelts (ZnO, SnO_2, In_2O_3, CdO, Ga_2O_3, and PbO_2) in 2001,[1] much effort has been made to beltlike nanostructures. Nanobelts with distinctive geometries present a good system for examining dimensionally confined and structurally well-defined chemical and physical phenomena.[2] They also have potential applications in nanoscale devices with diverse functions, mainly derived from the structural anisotropy and the low dimensionality combined with the quantum-confinement effect.[2–4] Up to date, some kinds of nanobelts based on metals (Ag, Au, and Ni),[5] nonmetallic elements (C, Si, and Te),[2a,6] oxides/hydrates (Fe_2O_3, Al_2O_3,VO_2(B), and $La(OH)_3$),[7] sulfides/selenides/tellurides/phosphides (ZnS, ZnSe, CdS, CdSe, and Sb_2Te_3),[8] carbide/nitrides (SiC and Si_3N_4),[9] and some complex compounds ($CuGeO_3$ and $Pb_3O_2Cl_2$),[10] etc., have been successfully fabricated with well-established techniques. Several novel properties have also been demonstrated.[7d,10a,b] Among various strategies, elegant hydrothermal process has shown an extraordinary ability in the low-temperature

* To whom correspondence should be addressed: Fax +86-027-67861185; e-mail liujp@phy.ccnu.edu.cn (J. Liu), xthuang@phy.ccnu.edu.cn (X. Huang).
† Central China Normal University.
‡ Hubei University.
§ Institute of Solid State Physics, Chinese Academy of Sciences.

(1) Pan, Z. W.; Dai, Z. R.; Wang, Z. L. *Science* **2001**, *291*, 1947.
(2) (a) Shi, W.; Peng, H.; Wang, N.; Li, C. P.; Xu; Lee, C. S.; Kalish, R.; Lee, S. T. *J. Am. Chem. Soc.* **2001**, *123*, 11095. (b) Yang, R.; Wang, Z. L. *J. Am. Chem. Soc.* **2006**, *128*, 1466.
(3) (a) Johnson, J. C.; Choi, H. J.; Knutsen, K. R.; Schaller, R. D.; Yang, P.; Saykally, R. J. *Nat. Mater.* **2002**, *1*, 106. (b) Yan, H.; Johnson, J.; Law, M.; He, R.; Knutsen, K.; McKinney, J. R.; Pham, J.; Saykally, R.; Yang, P. *Adv. Mater.* **2003**, *15*, 1907.
(4) (a) Wang, Z. L. *J. Phys.: Condens. Matter* **2004**, *16*, R829. (b) Comini, E.; Faglia, G.; Sberveglieri, G.; Pan, Z. W.; Wang, Z. L. *Appl. Phys. Lett.* **2002**, *81*, 1869.
(5) (a) Sun, Y.; Mayers, B.; Xia, Y. *Nano Lett.* **2003**, *3*, 675. (b) Zhang, J. L.; Du, J. M.; Han, B. X.; Liu, Z. M.; Jiang, T.; Zhang, Z. F. *Angew. Chem., Int. Ed.* **2006**, *45*, 1116. (c) Liu, Z.; Li, S.; Yang, Y.; Peng, S.; Hu, Z.; Qian, Y. *Adv. Mater.* **2003**, *15*, 1946. (d) Bai, J. W.; Qin, Y.; Jiang, C. Y.; Qi, L. M. *Chem. Mater.* **2007**, *19*, 3367.
(6) (a) Kang, Z.; Wang, E.; Mao, B.; Su, Z.; Gao, L.; Lian, S.; Xu, L. *J. Am. Chem. Soc.* **2005**, *127*, 6534. (b) Liu, J.; Shao, M.; Tang, Q.; Zhang, S.; Qian, Y. *J. Phys. Chem. B* **2003**, *107*, 6329. (c) Mo, M.; Zeng, J.; Liu, X.; Yu, W.; Zhang, S.; Qian, Y. *Adv. Mater.* **2002**, *14*, 1658.
(7) (a) Wen, X. M.; Wang, S. H.; Ding, Y.; Wang, Z. L.; Yang, S. H. *J. Phys. Chem. B* **2005**, *109*, 215. (b) Fang, X. S.; Ye, C. H.; Zhang, L. D.; Xie, T. *Adv. Mater.* **2005**, *17*, 1661. (c) Liu, J.; Li, Q.; Wang, T.; Yu, D.; Li, Y. *Angew. Chem., Int. Ed.* **2004**, *43*, 5048. (d) Hu, C.; Liu, H.; Dong, W.; Zhang, Y.; Bao, G.; Lao, C.; Wang, Z. L. *Adv. Mater.* **2007**, *19*, 470.
(8) (a) Ma, C.; Moore, D.; Li, J.; Wang, Z. L. *Adv. Mater.* **2003**, *15*, 228. (b) Yao, W. T.; Yu, S. H.; Pan, L.; Li, J.; Wu, Q. S.; Zhang, L.; Jiang, J. *Small* **2005**, *1*, 320. (c) Jiang, Y.; Meng, X. M.; Yiu, W. C.; Liu, J.; Ding, J. X.; Lee, C. S.; Lee, S. T. *J. Phys. Chem. B* **2004**, *108*, 2784. (d) Joo, J.; Son, J. S.; Kwon, S. G.; Yu, J. H.; Hyeon, T. *J. Am. Chem. Soc.* **2006**, *128*, 5632. (e) Shi, W.; Yu, J.; Wang, H.; Zhang, H. *J. Am. Chem. Soc.* **2006**, *128*, 16490. (f) Shen, G. Z.; Bando, Y.; Golberg, D. *J. Phys. Chem. C* **2007**, *111*, 5044.
(9) (a) Xi, G.; Peng, Y.; Wan, S.; Li, T.; Yu, W.; Qian, Y. *J. Phys. Chem. B* **2004**, *108*, 20102. (b) Shen, G. Z.; Bando, Y.; Liu, B. D.; Tang, C. C.; Huang, Q.; Golberg, D. *Chem.—Eur. J.* **2006**, *12*, 2987.
(10) (a) Song, R. Q.; Xu, A. W.; Yu, S. H. *J. Am. Chem. Soc.* **2007**, *129*, 4152. (b) Sigman, M. B.; Korgel, B. A. *J. Am. Chem. Soc.* **2005**, *127*, 10089. (c) Wang, J. W.; Li, Y. D. *Chem. Commun.* **2003**, 2320. (d) Mai, L. Q.; Lao, C. S.; Hu, B.; Zhou, J.; Qi, Y. Y.; Chen, W.; Gu, E. D.; Wang, Z. L. *J. Phys. Chem. B* **2006**, *110*, 18138. (e) Shi, H.; Qi, L.; Ma, J.; Wu, N. *Adv. Funct. Mater.* **2005**, *15*, 442. (f) Yu, J.; Yu, J. C.; Ho, W.; Wu, L.; Wang, X. *J. Am. Chem. Soc.* **2004**, *126*, 3422.

10.1021/cm702719s CCC: $40.75
Published on Web 12/12/2007

fabrication of beltlike nanostructures.[5c,7c,8e,10a] Very recently, Shen et al. reported on the first discovery of $Ag_2V_4O_{11}$ nanorings and microloops formed by the self-coiling of $Ag_2V_4O_{11}$ nanobelts under a hydrothermal process.[11] Their findings further confirmed the huge potentials of hydrothermal technique in shape control of nanomaterials. Despite much progress in this field, the design of new multicomponent nanobelts remains challenging to materials scientists.[10f] Research on nanobelts has been lagging far behind as compared to the significant achievements in nanowires and nanotubes.

Magnesium borate hydroxide ($MgBO_2(OH)$ or $2MgO\cdot B_2O_3\cdot H_2O$), also known as szaibelyite, is one kind of widely distributed translucent mineral in nature and the main source of boron in industry.[12] One of the most promising applications of szaibelyite is as precursor for the formation of anhydrous magnesium borates, which possess excellent mechanical properties and have applications in antiwear additives, thermoluminescence phosphor, ferroelastic materials, and electronic ceramics.[13,14] Recently, the thermochemistry of szaibelyite was studied, which is important for industrial application.[15] However, there are very few reports on the synthesis of nanostructured $MgBO_2(OH)$, although high-temperature processes (above 850 °C) have been successfully applied to the synthesis of anhydrous magnesium borates such as $Mg_3B_2O_6$ nanotubes,[16a] MgB_4O_7 nanowires,[16b] and $Mg_2B_2O_5$ nanowhiskers.[16c,d] In addition, the preparation of szaibelyite-related functional nanostructures such as long luminescent nanobelts has rarely been explored. Whereas, there is a growing interest in materials science for the development of new luminescence nanomaterials such as rare-earth-doped nanophosphors. Cheap and easily prepared host materials are highly demanded. It is expected that, after suitable surface-modification treatment with amino acids or biologically active molecules,[7d,17] the doped nanomaterials may be applied in the field of biolabeling. Also, nanoscale phosphors are expected to have medical applications such as phototherapy, optical image, and fluorescence resonance energy transfer (FRET) assays.[18] In addition, they exhibit certain properties that are superior to their bulk counterparts with respect to the application in transparent luminescent layers.[19] For example, they have higher packing density, better dispersion stability, and coating ability on the display panels. Eu^{3+}-doped red-light-emitting phosphors are of particular interest nowadays to researchers.[19] It is well-known that emission lines of Eu^{3+} ion correspond to transitions from the excited $^5D_0$ level to the ^7F_J ($J = 1, 2, ...$) levels of the $4f^6$ configuration. The orange emission in the range of 590–600 nm is due to the magnetic dipole transition $^5D_0 \rightarrow {}^7F_1$. The red emission around 610–630 nm is due to the electric dipole transition of $^5D_0 \rightarrow {}^7F_2$, induced by the lack of inversion symmetry at the Eu^{3+} site. A drawback of some Eu^{3+}-doped phosphors is the presence of an intense emission line in the orange region of the visible spectrum, so that the red emission color purity has to be improved. Searching for host materials that can supply the noncentrosymmetric site for Eu^{3+} is the key to obtain red phosphors with excellent color purity.[19f] To fulfill this demand, monoclinic $MgBO_2(OH)$ in which Mg^{2+} site has low local symmetry[12a] should be a good candidate.

In this paper, we present a facile hydrothermal process to synthesize $MgBO_2(OH)$ nanobelts, in the absence of any template or organic surfactant. The technique can be readily scaled up for multigram scale production (Supporting Information, Figure S1). More importantly, rare-earth Eu^{3+}-doped and Eu^{3+}, Y^{3+}-codoped nanobelts can also be achieved by a similar one-step process (120–180 °C) in high yield, for the first time. Optical studies indicate that $MgBO_2(OH)$ nanobelt is a good host material for highly luminescent nanostructures: cheap and lowly toxic. Intense pure red emission typical of Eu^{3+} ion is demonstrated. In addition, significant enhancement of the emission intensity (I_{em}) as well as the variation of the local crystal-field symmetry around Eu^{3+} induced by Y^{3+} codopant is observed. An attempt is also conducted to make these nanobelts into transparent thin film with uniform surface based on the mature coating technology.

2. Experimental Section

All chemicals were of analytical grade and were used without further purification. Doubly deionized water was used throughout. For the synthesis of pure $MgBO_2(OH)$ nanobelts, typically, $MgCl_2\cdot 6H_2O$ (2.03 g, 10 mmol) and KBH_4 (1.079 g, 20 mmol) were added separately in two glass beakers (50 mL capacity) containing water (25 mL) under stirring. After the addition, 25 min of ultrasonication was applied until two clear solutions were obtained. The concentrations of $MgCl_2$ and KBH_4 were about 0.4 and 0.8 M, respectively. The two solutions were further mixed and transferred into a Teflon-lined autoclave with a stainless-steel shell. The autoclave was kept at certain temperatures (120–180 °C) for 2 days and then allowed to cool to room temperature. The obtained precipitation was washed with pure ethanol and water several times to remove any other possible residues and then dried at 65 °C for

(11) Shen, G. Z.; Chen, D. *J. Am. Chem. Soc.* **2006**, *128*, 11762.
(12) (a) Takeuchi, Y.; Kudoh, Y. *Am. Mineral.* **1975**, *60*, 273. (b) Hawthorne, F. C. *Can. Mineral.* **1986**, *24*, 625.
(13) Liang, J. H. PhD Thesis, Tsinghua University, Beijing, China, 2005.
(14) Zhu, W.; Xiang, L.; He, T.; Zhu, S. *Chem. Lett.* **2006**, *35*, 1158.
(15) (a) Liu, Z. H.; Hu, M. C. *Thermochim. Acta* **2004**, *411*, 27. (b) Liu, Z. H.; Hu, M. C.; Gao, S. Y. *J. Therm. Anal. Calorim.* **2004**, *75*, 73. (c) Li, J.; Xia, S. P.; Gao, S. Y. *Spectrochim. Acta* **1995**, *51A*, 519.
(16) (a) Ma, R.; Bando, Y.; Golberg, D.; Sato, T. *Angew. Chem., Int. Ed.* **2003**, *42*, 1836. (b) Ma, R.; Bando, Y.; Sato, T. *Appl. Phys. Lett.* **2002**, *81*, 3467. (c) Li, Y.; Fan, Z. Y.; Lu, J. G.; Chang, R. P. H. *Chem. Mater.* **2004**, *16*, 2512. (d) Kitamura, T.; Sakane, K.; Wada, H. *J. Mater. Sci. Lett.* **1988**, *7*, 467.
(17) Wang, X.; Li, Y. D. *Angew. Chem., Int. Ed.* **2002**, *41*, 4790.
(18) (a) Dubertret, B.; Skourides, P.; Norris, D. J.; Noireaux, V.; Brivanloue, A. H.; Libchaber, A. *Science* **2002**, *298*, 1759. (b) Bühler, G.; Feldmann, C. *Angew. Chem., Int. Ed.* **2006**, *45*, 4864. (c) Meiser, F.; Cortez, C.; Caruso, F. *Angew. Chem., Int. Ed.* **2004**, *43*, 5954. (d) Kompe, K.; Borcher, H.; Storz, J.; Lobo, A.; Adam, S.; Moller, T.; Haase, M. *Angew. Chem., Int. Ed.* **2003**, *42*, 5513.
(19) (a) Wakefield, G.; Holland, E.; Dobson, P. J.; Hutchison, J. L. *Adv. Mater.* **2001**, *13*, 1557. (b) Kang, Y. C.; Roh, H. S.; Park, S. B. *Adv. Mater.* **2000**, *12*, 451. (c) Meyssamy, H.; Riwotzki, K.; Kornowski, A.; Naused, S.; Haase, M. *Adv. Mater.* **1999**, *11*, 840. (d) Wang, H.; Uehara, M.; Nakamura, H.; Miyazaki, M.; Maeda, H. *Adv. Mater.* **2005**, *17*, 2506. (e) Li, J.; Watanable, T.; Wada, H.; Setoyama, T.; Yoshimura, M. *Chem. Mater.* **2007**, *19*, 3592. (f) Tian, L. H.; Yu, B. Y.; Pyun, C. H.; Park, H. L.; Mho, S. *Solid State Commun.* **2004**, *129*, 43.

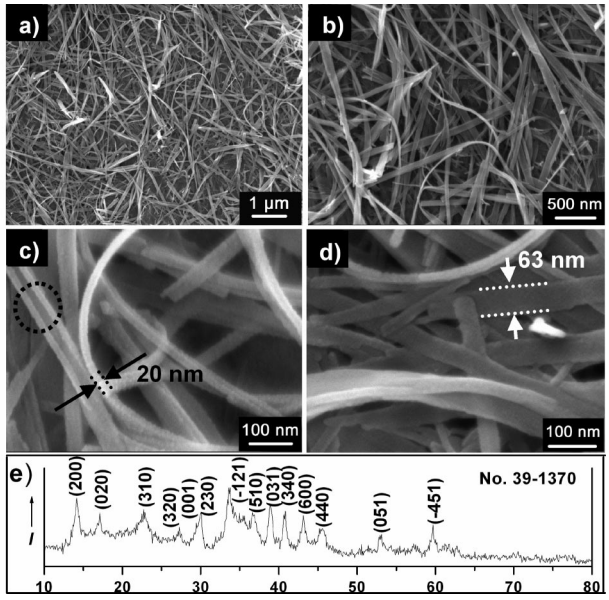

Figure 1. (a, b) SEM images and (c, d) high-magnification SEM images of as-synthesized $MgBO_2(OH)$ nanobelts. (e) XRD pattern.

5 h. For the fabrication of doped nanobelts, $Eu(NO_3)_3$ (0.1–1 mmol) [or $Eu(NO_3)_3$ (0.1–1 mmol) and $Y(NO_3)_3 \cdot 6H_2O$ (0.2 mmol)] was/were introduced before the above mixed solution was transferred into autoclave, and other experimental conditions were kept unchanged. The doping level was defined with respect to the molar quantity of Mg^{2+}.

The final products (over 94% yield, according to the amount of $MgCl_2 \cdot 6H_2O$ used) were collected for characterization. XRD experiments were conducted on a Bruker D-8 Avance X-ray diffractometer with Cu Kα radiation (λ = 1.5418 Å). The morphologies and structure were observed by FESEM (JSM-6700F; 5 kV) and TEM/HRTEM (JEM-2010FEF; 200 kV). The FT-IR spectrum was recorded on a NICOLET NEXUS470 Fourier transform infrared spectrometer. Thermogravimetric (TG) and differential thermal (DTA) analyses were carried out on an SDT600 apparatus with a heating rate of 10 °C min^{-1} in an air atmosphere. The excitation and emission spectra were recorded on a Perkin-Elmer LS-55 fluorescence spectrofluorometer at room temperature. For the test, a transparent colloidal solution of the nanobelts in ethanol was prepared by ultrasonication.

3. Results and Discussion

3.1. Synthesis of Pure $MgBO_2(OH)$ Nanobelts. Reaction between magnesium chloride hexahydrate ($MgCl_2 \cdot 6H_2O$) and potassium borohydride (KBH_4) at 120 °C in a sealed Teflon-lined stainless steel autoclave gave $MgBO_2(OH)$ nanobelts with high purity. Low-magnification field-emission scanning electron microscopy (FESEM) images (Figure 1a,b) show that the majority (>98%) of the as-prepared product is highly flexible nanobelts, with lengths of at least several tens of micrometers. The beltlike structure is further enlarged in Figure 1c,d, in which thickness and width of the appointed nanobelts can be determined to be 20 and 63 nm, respectively. In general, nanobelts are grown with typical widths of 30−100 nm and thickness in the range of 5–25 nm. Interestingly, some belts tend to roll up and form a tubular structure, as denoted by the circle in Figure 1c. An X-ray diffraction (XRD) pattern of the obtained product is shown

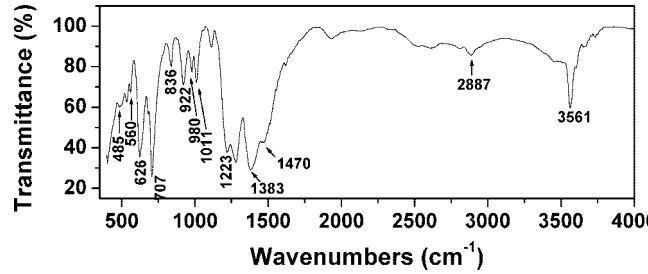

Figure 2. FT-IR spectrum of the as-prepared nanobelts.

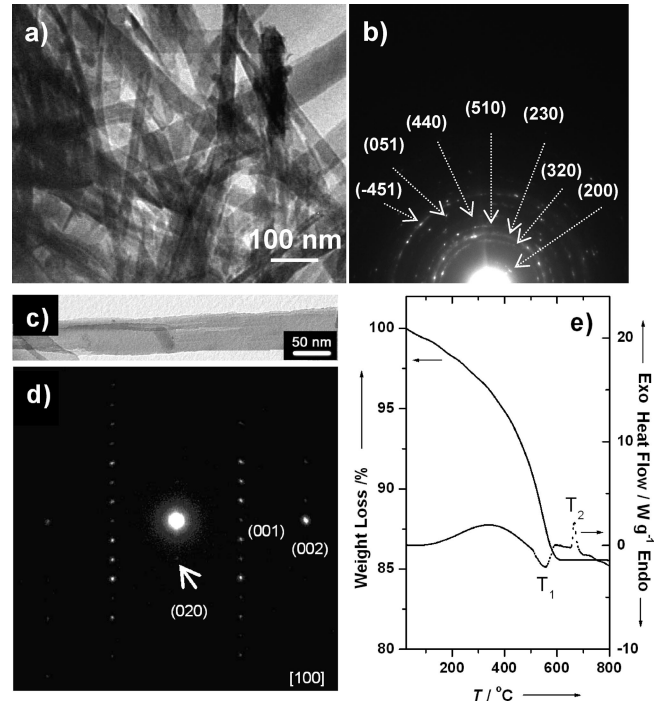

Figure 3. (a) TEM image and (b) diffraction pattern of a number of nanobelts. (c) TEM image and (d) SAED result of an individual nanobelt. (e) TG and DTA analyses of the as-prepared nanobelts.

in Figure 1e. All peaks can be perfectly indexed as the pure monoclinic phase (Joint Committee on Powder Diffraction Standards (JCPDS) File Card No. 39-1370) of $MgBO_2(OH)$. Fourier transform infrared (FT-IR) spectroscopy analysis also confirms the composition of product. As indicated in Figure 2, the characteristic peaks of $MgBO_2(OH)$ at 485 cm^{-1} (bending mode of B(4)−O), 560 cm^{-1} (in-plane bending of B(3)−O), 626 cm^{-1} (symmetric pulse vibration of $[B_2O_4(OH)_2]^{4-}$), 707 cm^{-1} (out-of-plane bending of B(3)−O), 836 cm^{-1}(symmetric stretching of B(4)−O), 1011 cm^{-1} (asymmetric stretching of B(4)−O), and 1223 cm^{-1} (in-plane bending of B−O−H) are observed.[15c] The bands at 1470, 1383 cm^{-1} and 980, 922 cm^{-1} might be the asymmetric and symmetric stretching of B(3)−O, respectively. The bands at 3561 and 2887 cm^{-1} are the stretching of O−H and the O−H stretching mode of the strong hydrogen bond, respectively.[15c]

The nanobelts were further characterized by transmission electron microscopy (TEM). Figure 3a shows the TEM image of a number of nanobelts. The selected-area electron diffraction (SAED) result obtained by focusing an electron beam onto these belts is illustrated in Figure 3b. From the pattern, the reflections of (200), (320), (230), (510), (440), (051),

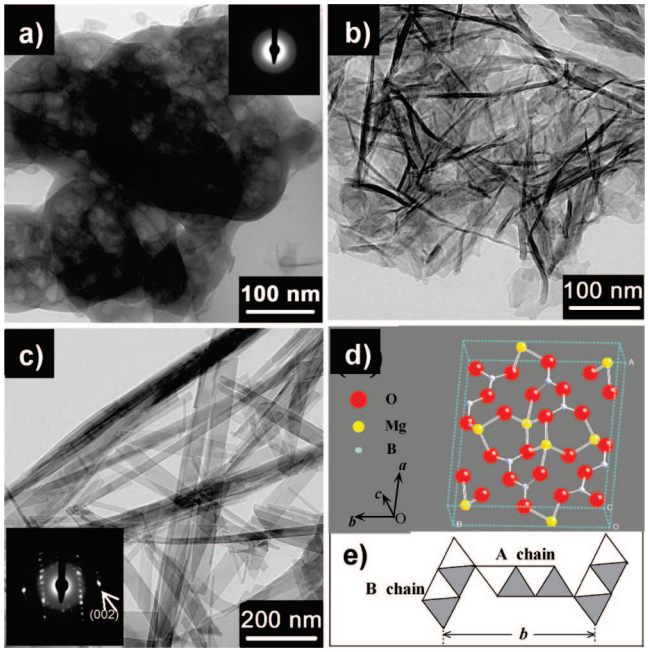

Figure 4. TEM images and corresponding SAED patterns (insets) of the products obtained at reaction times of (a) 30 min, (b) 2 h, and (c) 18 h. (d) An atomic model of szaibelyite (hydrogen is not included). (e) Schematic diagram showing the single octahedral sheet formed by A and B chains; projection along the *c* axis.

and (−451) planes can be identified, indicating that the products are crystalline $MgBO_2(OH)$ composed of many single crystal nanobelts. A typical TEM image of an individual nanobelt is also shown in Figure 3c. The SAED pattern (Figure 3d) taken from different parts along the belt is similar and can be indexed as a monoclinic $MgBO_2(OH)$ single crystal with a [001] growth direction. The wide and side surfaces of the nanobelt are easily determined to be {200} and {020}, respectively. The nanobelts are very sensitive to electron beam illumination, and the structure is rapidly damaged and is transformed to amorphous component when we try to obtain the high-resolution TEM (HRTEM). Consistent with this result, thermogravimetric (TG) analysis indicates that the as-prepared nanobelts have a rapid weight loss at 550 °C. Differential thermal analysis (DTA) in Figure 3e shows that there are two main peaks: one endothermic peak centered at 550 °C corresponds to the loss of water molecules and dehydroxylation, leading to the formation of amorphous $Mg_2B_2O_5$; the other exothermic peak at 664 °C with no associated weight loss corresponds to the recrystallization of $Mg_2B_2O_5$. As a consequence of this process, XRD of the calcinated sample is consistent with crystallized $Mg_2B_2O_5$ (Supporting Information, Figure S2a).

3.2. Shape Evolution and Growth Mechanism. Figure 4a−c shows TEM pictures depicting the structural evolution with reaction time (also see Supporting Information, Figure S2b−d). Amorphous foamlike structure was first obtained after 30 min reaction (Figure 4a and its inset SAED). Thin and flexible flakes were formed after 2 h (Figure 4b) and further grew with time, forming a flake-belt coexisted product after 10 h. Beltlike structures appeared at the cost of the thin flakes; as a result, pure and short nanobelts can be attained after 18 h of reaction, with a nearly single-crystal structure (Figure 4c). A further increase in the time led to the formation of long nanobelts. It was also found that the foam- and flakelike structures were $Mg_7B_4O_{13}\cdot 7H_2O$, different from the composition of nanobelts ($MgBO_2(OH)$). On the basis of the above process and our experimental steps, the formation of such belts involves the first growth of $Mg_7B_4O_{13}\cdot 7H_2O$ nanoflakes and their subsequent dissolution, reaction, and the final recrystallization of $MgBO_2(OH)$. The main chemical reactions are as follows:

$$BH_4^- + 4H_2O \rightarrow H_3BO_3 + 4H_2 + OH^- \quad (1)$$

$$7Mg^{2+} + 4H_3BO_3 + 14OH^- \rightarrow Mg_7B_4O_{13}\cdot 7H_2O + 6H_2O \quad (2)$$

$$Mg_7B_4O_{13}\cdot 7H_2O + 3H_3BO_3 \rightarrow 7MgBO_2(OH) + 8H_2O \quad (3)$$

Simply, the overall reaction can be formulated as shown in eq 4.

$$2BH_4^- + Mg^{2+} + 6H_2O \rightarrow MgBO_2(OH) + 8H_2 + H_3BO_3 \quad (4)$$

This typical dissolution−recrystallization process has been extensively observed in hydrothermal synthesis of anisotropic nanostructures.[5c,11,17,20] Our control experiments indicated that, in the temperature range of 120–180 °C, the growth of single-crystal nanobelts was not greatly affected by the reaction temperature; nanobelts with similar size and structure were produced. However, the concentration of KBH_4 was a key parameter to fabricate $MgBO_2(OH)$ nanobelts in large quantities. The optimum concentration was determined as 0.7–0.9 M. Herein, when the concentration was decreased, for example, to 0.4 M which is less than stochiometric according to eq 4, the products were dominated by $Mg_7B_4O_{13}\cdot 7H_2O$ nanosheets (Figure 5). On the other hand, at high concentration of KBH_4 (>1.0 M), excessive OH^- and H_3BO_3 were produced by the hydrolyzation of KBH_4, which significantly changed the chemical environment in solution. In that case, less precipitation of $MgBO_2(OH)$ nanobelts was obtained. We also found that additional acid and alkali were not beneficial to the formation of nanobelts. For instance, the products fabricated by the introduction of additional 0.8 g of NaOH under otherwise similar conditions were pure $Mg(OH)_2$ hexagonal nanodisks (Supporting Information, Figure S3). In the present study, it is worth pointing out that nanobelts can be fabricated in mild solution without using any organic surfactant. This is quite different from many previous works,[5b,c,8e,20] in which organic additives were used to selectively adsorb onto the crystallographic planes of inorganic materials, thus serving as directing agents and kinetically controlling the anisotropic growth of them.

As for the reason for the formation of nanobelts, the bulk crystal structure of szaibelyite should be considered. Figure 4d illustrates an atomic model of szaibelyite. The structure consists of distorted Mg−O octahedra which share edges to

(20) Ye, C. H.; Bando, Y.; Shen, G. Z.; Golberg, D. *Angew. Chem., Int. Ed.* **2006**, *45*, 4922.

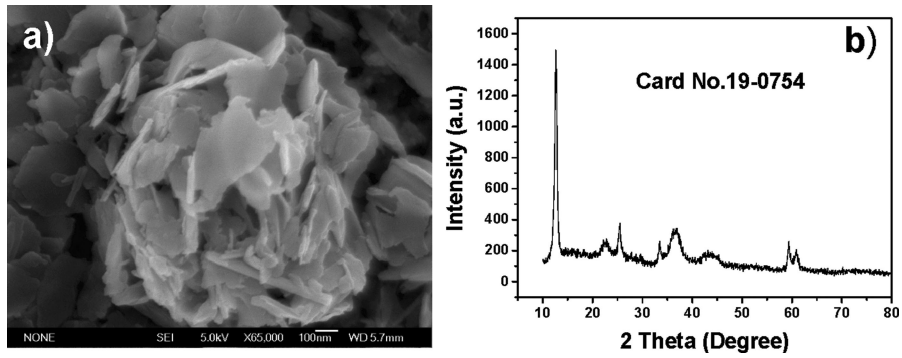

Figure 5. (a) SEM image and (b) XRD result of the product synthesized by using 0.4 M $MgCl_2$ and 0.4 M KBH_4 (120 °C, 48 h). The product is $Mg_7B_4O_{13}\cdot 7H_2O$.

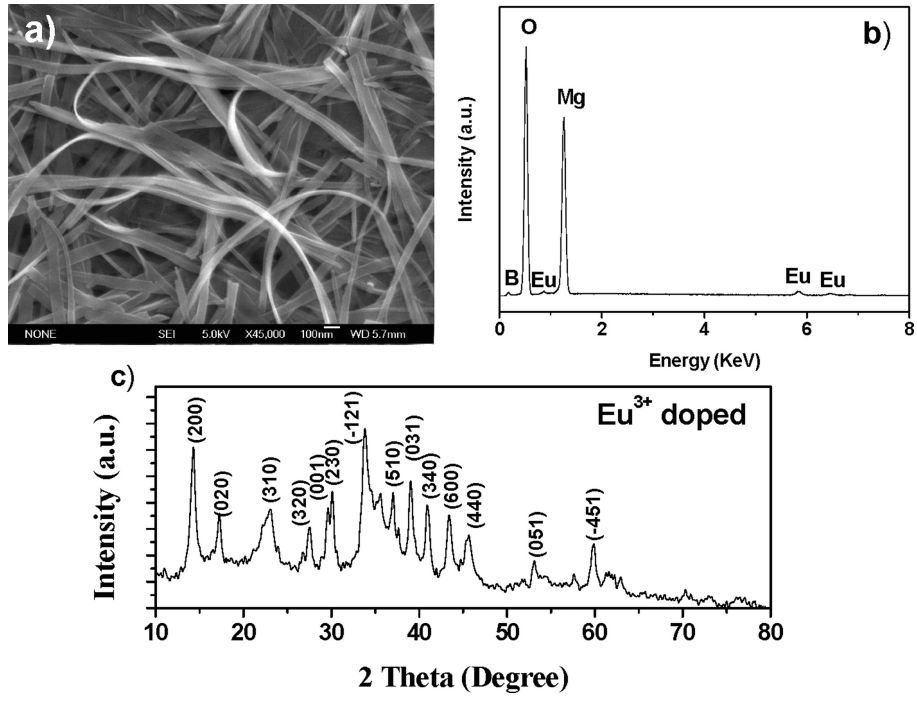

Figure 6. (a) SEM image of 5% Eu^{3+}-doped $MgBO_2(OH)$ nanobelts. (b) EDS result showing the existence of Eu element. In addition, the molar ratio of Mg to Eu is close to that employed in the synthesis. (c) XRD result of the doped nanobelts.

form a chain, two octahedra in width, parallel to the *c* axis. Two such nonequivalent chains, A chain and B chain (Figure 4e), share corners to form a sheet parallel to (200). The sheets are further held together by pyroborate ions $[B_2O_4(OH)]^{3-}$.[12a] This special crystallographic structure readily endows $MgBO_2(OH)$ nanostructures with a sheetlike shape with (200) as the wide surface. In addition, it is believed that the ultimate morphology of $MgBO_2(OH)$ is determined by different growth rates of crystal faces. According to the Bravais−Friedel−Donnay−Harker (BFDH) law,[21] the growth rate of such a crystal is normally proportional to $1/d_{hkl}$. Thus, nanobelts grow along [001] direction mainly because that the interplanar distance of (002) plane is smaller than those of (020) and (200) planes. Under hydrothermal conditions, the growth along *c* axis can be further accelerated, and this will also contribute to the final formation of long nanobelts. As mentioned above, some rolled-up $MgBO_2(OH)$ structures can be detected in the product fabricated at 120 °C. We attempted to fabricate well-defined $MgBO_2(OH)$ nanotubes based on this interesting phenomenon, by conducting the experiment at higher temperature (180–250 °C) or prolonging the reaction time. However, unlike previous report on $SrAlO_4$,[20] nanobelts in our study were not further rolled up and developed into nanotubes. One possible reason is that thermal energy actually could not overcome the potential energy barrier associated with the induced strain by rolling up $MgBO_2(OH)$ under these conditions. Otherwise, chemical environment may contribute to this since the occurrence of rolled-up nanoscrolls also depends on the chemical environments such as the pH and ionic strength.[22]

3.3. Synthesis and Optical Properties of Doped Nanobelts. With the introduction of europium ions (Eu^{3+}) into the reaction solution, Eu-doped $MgBO_2(OH)$ ($MgBO_2(OH)$:Eu^{3+}) nanobelts can be successfully synthesized, evidenced by the SEM, XRD, and energy-dispersed X-ray spectrometer (EDS) experiments (Figure 6a−c). Note that the high water solubility of the starting materials facilitated the ion exchange/

(21) Hartman, P.; Perdok, W. G. *Acta Crystallogr.* **1955**, *8*, 49.

(22) (a) Saupe, G. B.; Waraksa, C. C.; Kim, H. N.; Han, Y.; Kaschak, M. D.; Skinner, D. M.; Mallouk, T. E. *Chem. Mater.* **2000**, *12*, 1556. (b) Schaak, R. E.; Mallouk, T. E. *Chem. Mater.* **2000**, *12*, 3427.

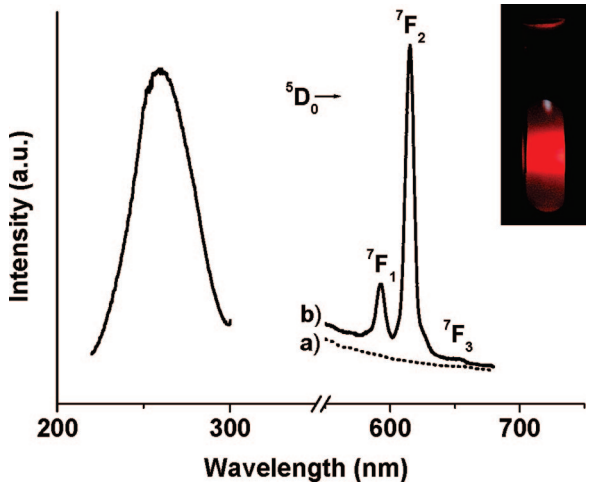

Figure 7. Excitation spectrum (left, $\lambda_{em} = 615$ nm) and emission spectra ($\lambda_{ex} = 260$ nm) of the as-synthesized pure $MgBO_2(OH)$ nanobelts (right (a)) and $MgBO_2(OH)$:5%Eu^{3+} nanobelts (right (b)). Experimental temperature: 180 °C. Inset shows the red luminescence from the doped sample recorded with a digital camera.

transport and the doping process. As shown in Figure 6a, the typical width and thickness of 5% Eu^{3+}-doped nanobelts are similar to those of pure ones. However, the XRD analysis (Figure 6c) shows slight shifts to the large 2θ value in the position of the diffraction peaks, as compared to the result of pure nanobelts. For instance, the lattice spacing d values corresponding to peaks of (200), (020), and (310) can be calculated to be 6.196, 5.1457, and 3.8818 Å, respectively, for doped nanobelts and 6.322, 5.2358, and 3.9392 Å, respectively, for pure nanobelts. It is obvious that the d values have decreased after doping. When tervalent Eu^{3+} ions are successfully doped into $MgBO_2(OH)$ host materials, they replace the positions of bivalent Mg^{2+}. In order to maintain the charge neutrality, some negatively charged defects are readily generated in the crystal lattice, resulting in the lattice deformation and thus the decrease of d values.

The excitation and emission spectra of $MgBO_2(OH)$:5%Eu^{3+} nanobelts (180 °C, 48 h) are illustrated in Figure 7. The broad band with the maximum value at 260 nm in the excitation spectrum is attributed to a charge-transfer transition, which occurs by electron delocalization from the filled 2p shell of the O^{2-} in $MgBO_2(OH)$ to the partially filled 4f shell of Eu^{3+}.[23] The emission spectrum (Figure 7b) consists of three main peaks between 550 and 675 nm, which correspond to the $^5D_0 \rightarrow {}^7F_J$ transitions of Eu^{3+} ($^5D_0 \rightarrow {}^7F_1$ at 593 nm; $^5D_0 \rightarrow {}^7F_2$ at 615 nm; $^5D_0 \rightarrow {}^7F_3$ at 654 nm).[19a,c,d,24] It is worth mentioning that pure nanobelts could not emit any luminescence (Figure 7a). In contrast, the as-created $MgBO_2(OH)$:

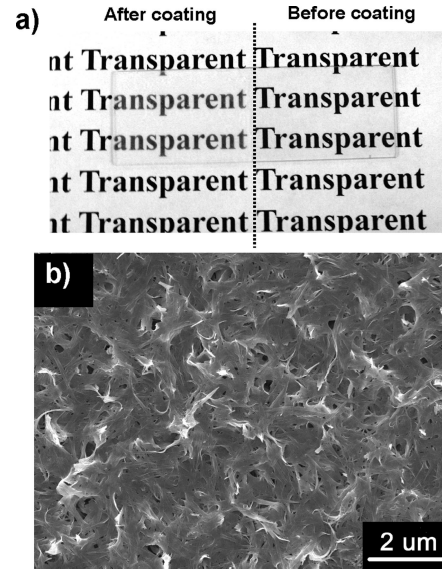

Figure 8. (a) Photograph of a glass coated with $MgBO_2(OH)$ nanobelts, showing that the nanobelts can be easily made into transparent film. (b) A typical SEM image of the film, which demonstrates that nanobelts are uniform and densely packed.

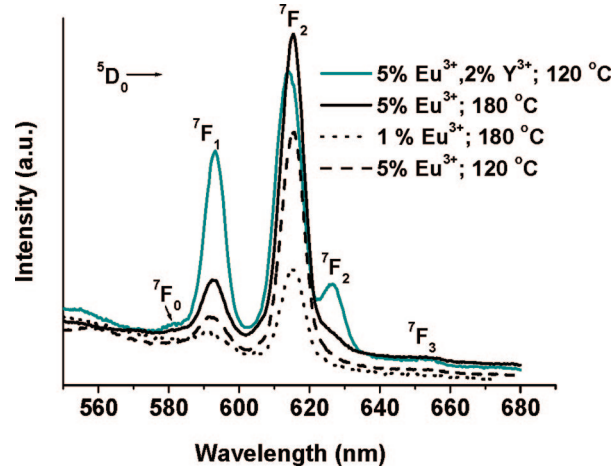

Figure 9. Emission spectra ($\lambda_{ex} = 260$ nm) of doped $MgBO_2(OH)$ nanobelts synthesized under different conditions.

5%Eu^{3+} nanobelts exhibit a strong red emission (Figure 7, inset) that is visible to the naked eye. The dominant 615 nm emission, typically observed from the well-known Y_2O_3:Eu and zircon-type $LaVO_4$:Eu phosphors,[19a,b,d,24b,d] is crucial to potential applications with the demand of high red-color purity.[24d] In this regard, our low-cost beltlike $MgBO_2(OH)$ is superior to many reported rare-earth element containing host materials such as $LaPO_4$,[19c] YBO_3,[24a] and $Y_2Sn_2O_7$,[25] since for these materials, the I_{em} of the $^5D_0 \rightarrow {}^7F_2$ transition was usually lower than that of the $^5D_0 \rightarrow {}^7F_1$ transition. In addition, the as-prepared doped nanobelts can be easily made into transparent thin film by a simple coating method, endowing them with practical application in displays (Figure 8a). A typical SEM image in Figure 8b illustrates that the film is uniform, consisting of densely packed nanobelts. Further in-depth study demonstrates that the I_{em} increases with an increase in Eu^{3+} concentration. As an example, the I_{em} of the 5% Eu^{3+}-doped $MgBO_2(OH)$ nanobelts is appar-

(23) Blasse, G.; Grabmaier, B. C. *Luminescent Materials*; Springer: Berlin, 1994.

(24) (a) Jiang, X. C.; Sun, L. D.; Yan, C. H. *J. Phys. Chem. B* **2004**, *108*, 3387. (b) Jia, C. J.; Sun, L. D.; Luo, F.; Jiang, X. C.; Wei, L. H.; Yan, C. H. *Appl. Phys. Lett.* **2004**, *84*, 5305. (c) Liu, J. F.; Li, Y. D. *Adv. Mater.* **2007**, *19*, 1118. (d) Wei, Z. G.; Sun, L. D.; Liao, C. S.; Yan, C. H.; Huang, S. H. *Appl. Phys. Lett.* **2002**, *80*, 1447. (e) Yan, R. X.; Sun, X. M.; Wang, X.; Peng, Q.; Li, Y. D. *Chem.—Eur. J.* **2005**, *11*, 2183. (f) Yu, M.; Lin, J.; Fang, J. *Chem. Mater.* **2005**, *17*, 1783. (g) Karmaoui, M.; Ferreira, R. A. S.; Mane, A. T.; Carlos, L. D.; Pinna, N. *Chem. Mater.* **2006**, *18*, 4493. (h) Zhao, F.; Yuan, M.; Zhang, W.; Gao, S. *J. Am. Chem. Soc.* **2006**, *128*, 11758. (i) Wu, C. C.; Chen, K. B.; Lee, C. S.; Chen, T. M.; Cheng, B. M. *Chem. Mater.* **2007**, *19*, 3278.

(25) Fujihara, S.; Tokumo, K. *Chem. Mater.* **2005**, *17*, 5587.

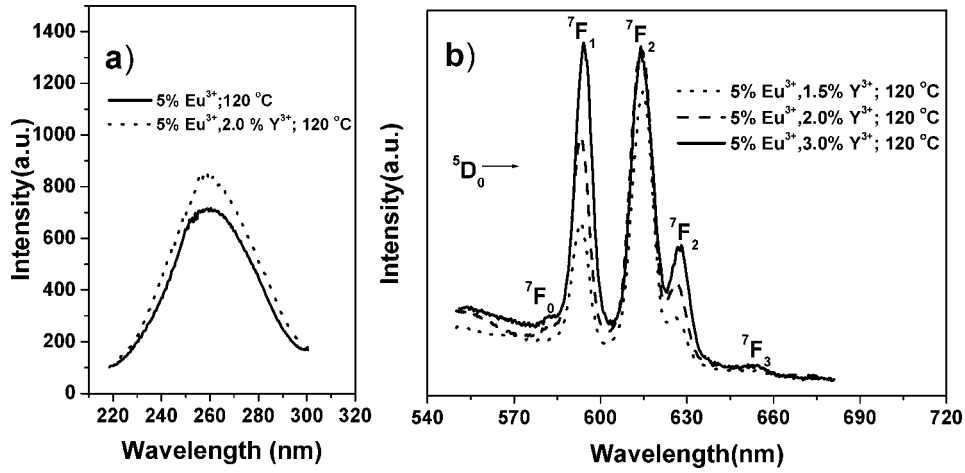

Figure 10. (a) Excitation spectra of $MgBO_2(OH)$:5%Eu^{3+} and $MgBO_2(OH)$:5%Eu^{3+}, 2%Y^{3+} nanobelts fabricated at 120 °C ($\lambda_{em} = 615$ nm). (b) Emission spectra of $MgBO_2(OH)$ nanobelts codoped with 5% Eu^{3+} and Y^{3+} of different concentrations ($\lambda_{ex} = 260$ nm).

ently higher than that of the 1% doped nanobelts (Figure 9). Nevertheless, beyond 5 mol % doping, the emission tends to be quenched because of the multipole−multipole and/or the superexchange interaction between the Eu^{3+} ions. The reaction temperature also has influence on the I_{em}; a sample prepared at 120 °C exhibits relatively weak emission. It is generally believed that luminescence intensity of nanostructured materials is in many cases reduced by defects and surface groups at the interface. Thus, higher I_{em} could probably be achieved if residual crystalline defects and nonradiative relaxations from surface groups are well controlled.[18d,19d,24g,h]

Benefiting from the facile reaction process, codoped nanobelts can be further achieved. By introducing another rare-earth ion, the emission property changes accordingly. As shown in Figure 9, the emissions of $MgBO_2(OH)$:5%Eu^{3+}, 2%Y^{3+} and $MgBO_2(OH)$:5%Eu^{3+} nanobelts are compared (both were synthesized at 120 °C). It is apparent that the introduction of Y^{3+} leads to the appearance of two new peaks at 580 and 626 nm, corresponding to $^5D_0 \rightarrow {}^7F_0$ and $^5D_0 \rightarrow {}^7F_2$ transitions of Eu^{3+}, respectively; moreover, the I_{em} of all the peaks are enhanced. Despite this, the peak positions are only related to Eu^{3+} activators. A significant spectral change caused by Y^{3+} doping is the increase of intensity ratio (R) of 593 to 615 nm emissions. As is well-known, R mainly depends on the local symmetry of the crystal field of the Eu^{3+}.[19a,24d,f] The increased R value indicates a higher symmetry of crystal field around Eu^{3+}. In monoclinic phased $MgBO_2(OH)$:Eu (space group: $P2_1/a$), Eu^{3+} occupies the Mg^{2+} site and is surrounded by six oxygen ions, forming a distorted octahedron. Obviously, for $MgBO_2(OH)$:Eu nanobelts, the red emission at 615 nm from the transition $^5D_0 \rightarrow {}^7F_2$ (a electric dipole transition) should be dominant due to this low local symmetry (without inversion center). After the introduction of Y^{3+}, the orange emission (593 nm) from $^5D_0 \rightarrow {}^7F_1$ transition (a magnetic dipole transition) is no longer strictly forbidden. The reason for this interesting phenomenon is now not fully understood and needs further investigation. Nevertheless, it is speculated that new crystal field bonding sites for Eu^{3+} can be generated (such as the appearance of Eu−O−Y linkages[26]) by codoping, which may change the environment of Eu^{3+} from a site lacking inversion symmetry to one of relatively near inversion symmetry. The emergence of $^5D_0 \rightarrow {}^7F_0$ transition of Eu^{3+} (which is only allowed for C_s, C_n, and C_{nv} symmetry[24e,f]) is an evidence for the variation of crystal field symmetry. Furthermore, the charge compensation effect should be considered. When Y^{3+} ions further replace the Mg^{2+} sites in the lattice, more defects such as oxygen interstitials and displacements have to be introduced to compensate for the change in charge. Too many defects generated in crystal lattice for the charge compensation will cause lattice distortion and facilitate the change of crystal field symmetry. Previously, the effect of modifying cations on the emission property of sol–gel SiO_2:Eu was reported on the basis of fluorescence line-narrowing spectroscopy.[26] As suggested, codopants such as Y^{3+} could inhibit the clustering of Eu^{3+}. However, the enhancement of I_{em} was not observed and discussed. It is well-known that Eu^{3+} clusters are commonly formed in single-doped systems. This clustering can lead to fast energy transfer, luminescence quenching, and lifetime shortening. In our work, the way Y^{3+} ions inhibit the clustering of Eu^{3+} is to penetrate them. This is reasonable because Y^{3+} ions have similar ionic radius and the same valence state to Eu^{3+}.[25] Since Y^{3+} may penetrate Eu^{3+} clusters, the average Eu^{3+}−Eu^{3+} distance increases. In principle, this will lead to lower concentration quenching and thus the increase of I_{em}. On the other hand, we find that the absorption of 260 nm UV light can also be enhanced by the introduction of 2% Y^{3+}. As illustrated in Figure 10a, $MgBO_2(OH)$:5%Eu^{3+}, 2%Y^{3+} nanobelts exhibit stronger absorption than $MgBO_2(OH)$:5%Eu^{3+} nanobelts. In $MgBO_2(OH)$ lattice, electrons of oxygen in borate anions are typically bound to Mg^{2+}.[12a] When nanobelts are codoped, this restriction will be weakened because of Y^{3+} incorporation. Thus, the electron transition from the filled 2p shell of the O^{2-} to the partially filled 4f shell of Eu^{3+} occurs more easily, resulting in the intensity increase in absorption. The absorption enhancement undoubtedly contributes to the increase of the overall emission intensity. Herein, we explicitly provide

(26) Costa, V. C.; Lochhead, M. J.; Bray, K. L. *Chem. Mater.* **1996**, *8*, 783.

evidence for the intensity enhancement caused by Y^{3+} incorporation. Specially, this effect seems to be very significant in our system for the concentration of Y^{3+} we used is far lower than that in ref 26, which should be strongly related to the nature of $MgBO_2(OH)$ host material. It is proposed that the Y^{3+}-induced intensity improvement can be utilized as an efficient means to improve the performance of Eu^{3+}-doped nanophosphors. By this means, the degree of intensity enhancement will be easily controlled by the quantity of Y^{3+}. To clarify this, the emission spectra of $MgBO_2(OH)$ nanobelts codoped with 5% Eu^{3+} and Y^{3+} of two different concentrations (1.5% and 3%) were further examined, and the comparative results are shown in Figure 10b. As can be seen, the overall emission intensity, especially the intensity of peak at 593 nm, can be gradually enhanced with the increase of Y^{3+} concentration.

4. Conclusions

In summary, we have developed a convenient hydrothermal process to synthesize pure, doped, and codoped $MgBO_2(OH)$ nanobelts on a large scale. Our work represents an example of fabricating doped magnesium borates at very low temperatures, which enables a flexible control over particle size/shape and the degree of agglomeration. The pure nanobelts can be used as building blocks to form a variety of functional nanostructures with special physical and chemical properties. The Eu^{3+}-doped nanobelts with low toxicity show efficient red emission dominated at 615 nm and can be readily made into transparent thin film, indicating that they are good candidates for transparent luminescent layers and other potential optical devices. It is feasible that the environmentally benign method presented herein will be of great potential for the generation of other multicomponent functional nanobelts with or without dopants.

Acknowledgment. We gratefully acknowledge financial support from the National Natural Science Foundation of China (No. 50202007). We are appreciative of the valuable suggestions from the reviewers for the revision of this paper.

Supporting Information Available: Photograph of the powder of $MgBO_2(OH)$ nanobelts; XRD of heated and intermediate products; SEM results of intermediate products; SEM and XRD results of the product attained by the introduction of 0.8 g of NaOH. This material is available free of charge via the Internet at http://pubs.acs.org.

CM702719S